Template-Aluminosilicate Structures at the Early Stages of Zeolite ZSM-5 Formation. A Combined Preparative, Solid-state NMR, and Computational Study

Pieter C. M. M. Magusin,*,† Vadim E. Zorin,†,§ Alexander Aerts,‡ Christophe J. Y. Houssin,†,§ Alexei L. Yakovlev,†,§ Christine E. A. Kirschhock,‡ Johan A. Martens,‡ and Rutger A. van Santen†

Schuit Institute of Catalysis, Eindhoven University of Technology, The Netherlands, and Centre for Surface Chemistry and Catalysis, Catholic University Leuven, Belgium

Received: June 15, 2005; In Final Form: October 7, 2005

Species at three stages in the self-assembly of zeolite ZSM-5 have been studied with one- and two-dimensional magic-angle-spinning ^{13}C, ^{27}Al, ^{29}Si, and ^{1}H NMR spectroscopy and compared with the earlier proposed structures: (1) precursor species containing 33−36 T sites around a tetrapropylammonium (TPA) cation, (2) nanoslabs consisting of a flat 4 × 3 array of such precursors, and (3) the final TPA-ZSM-5 zeolite. Synthesis was carried out in D_2O to suppress the water and silanol protons. Under such conditions, the effective Si−H and Al−H distances measured with ^{29}Si-{^{1}H} and ^{27}Al-{^{1}H} rotational echo double resonance (REDOR) reflect the interactions between TPA cations and the surrounding aluminosilica. The ^{29}Si-{^{1}H} REDOR curves for Q^4-type silicon atoms at the three mentioned stages are closely similar, as well as the observed $^{27}Al-^{1}H$ REDOR curve for the precursor species compared to that for the TPA-ZSM-5. This indicates that in addition to externally attached TPA, there is also internal TPA already incorporated at an early stage into the aluminosilicate in a similar way as in the final zeolite, in accordance with the earlier proposed MFI self-assembly pathway (Kirschhock et al. *Angew. Chem. Int. Ed.* **2001**, *40*, 2637). However, the effective distances extracted from the initial REDOR curvatures are significantly (10−15%) larger than those computed for the model. Since there is no temperature effect, we tentatively assign this difference to a reduction of the $^{29}Si-^{1}H$ and $^{27}Al-^{1}H$ interactions by multispin decoherence effects or self-decoupling caused by proton spin diffusion. By assuming the computed model distances and fitting Anderson−Weiss curves to the observed REDOR data, we obtain similar "decoherence times" in the order of 0.1 ms. The observed ^{29}Si-{^{1}H} REDOR dephasing for the Q^3 sites in the precursors is significantly faster than that for the Q^4 sites. This is tentatively ascribed to a partial deuteron−proton back exchange at the silanol positions.

Introduction

Tetrapropylammonium (TPA) cations are effective templates for the synthesis of silicalite-1, a crystalline silica molecular sieve with MFI framework topology.[1] Several groups have investigated the role of TPA at the early stages of silicalite-1 formation. Analysis by ion exchange and neutron scattering of hydrogels, obtained from TPA−OH and various silicon sources, indicates TPA incorporation into the gel particles in environments similar to the final zeolite.[2,3] The short-range intermolecular TPA−silicate interactions were examined by use of $^{1}H-^{29}Si$ and $^{1}H-^{13}C$ cross-polarization (CP) magic-angle-spinning (MAS) NMR on selectively deuterated gels.[4] Efficient polarization transfer from the TPA protons to silicon atoms was observed proving that TPA is embedded at the van der Waals length scale into the silicate network even before long-range crystalline order arises. The conformation and the confinement of these TPA molecules resemble their position in channel intersections of crystalline TPA-ZSM-5.

In the clear-solution synthesis of silicalite-1,[5] the reaction of TPA−OH with the silicon source at room temperature yields a transparent suspension of subcolloidal particles. The absence of a gel phase facilitates the study of emerging silicate species. Primary particles with well-defined characteristic lengths between 2 and 5 nm were identified using SAXS,[6−11] SANS,[8] DLS,[12−15] and HRTEM[6,12−14] depending on the preparation of the clear solution. The subcolloidal particles were believed to be amorphous aggregates of TPA−silica clathrates[6,7,10,11] or entities already possessing characteristics of the silicalite-1 structure based on investigations with SANS, FTIR, Raman spectroscopy, electron diffraction, and nitrogen adsorption.[8,9,15−17] The latter assumption was confirmed and further developed into a detailed structural model[18−20] and mechanism of formation[21] of these subcolloidal particles, proposed by Kirschhock and Ravishankar et al. The subcolloidal particles were found to have the MFI framework topology with a TPA molecule in each of the channel intersections.[16] These slab-shaped 1.3 × 4 × 4 nm polysilicate units were termed nanoslabs. ^{29}Si NMR, GPC, and SAXS measurements led to the identification of a 33−36 Si-atom polysilicate precursor of the nanoslab. Liquid-state ^{29}Si NMR has shown how the precursor itself is selectively formed through cluster−cluster aggregation of specific silicate oligo-

* To whom correspondence should be addressed. E-mail: p.c.m.m.magusin@tue.nl; Address: P.O. Box 513, 5600 MB Eindhoven, The Netherlands.

† Eindhoven University of Technology.

‡ Catholic University of Leuven.

§ Current addresses: V. E. Zorin, Department of Chemistry, Durham University, South Road, Durham, DH1 3LE, U. K.; C. J. Y. Houssin, BASF Aktiengesellschaft Forschung Katalyse Industriekatalysatoren GCC/I-M301 67056 Ludwigshafen, Germany; A. L.Yakovlev Theoretical Chemistry, Vrije Universiteit Amsterdam, The Netherlands.

10.1021/jp053217u CCC: $30.25
Published on Web 11/11/2005

mers. The precursor with the MFI framework connectivity contains one hydrophobic TPA molecule, shielded from the aqueous reaction mixture by the hydrophobic inner silica surface of the precursor. Aggregation of 12 precursors results in a nanoslab. However, the detailed synthesis mechanism is still under debate, in particular the role of the TPA cations. Knight and Kinrade claim a cubic octameric silicate polyanion to be the dominant equilibrium species in aqueous tetraalkylammonium solutions which is too small to accommodate a TPA cation.[22,23] They state that the hydrated organic cations encapsulate the silicate anion in solution and not *vice versa* as proposed by the nanoslab precursor model. Others have also proposed silica nanoparticles with externally attached TPA at early stages in the synthesis.[24,25]

To contribute to this discussion, we have investigated three systems representing various stages in the MFI synthesis pathway, namely, freeze-dried precursor powder (1), frozen solution of nanoslab (2), and uncalcined zeolite ZSM-5 still containing the TPA cations (3) with various solid-state NMR techniques. As a novel element in the NMR investigation of MFI self-assembly, the studied systems contain a small amount of aluminum-substituting silicon (Si/Al = 50). The first reason for this is that the Brønsted acidic ZSM-5 is more frequently used in industrial applications than the purely siliceous silicalite. The second reason is that ^{27}Al is a convenient NMR nucleus with quadrupolar properties and, therefore, with a NMR line shape reflecting the local charge distribution. It is still in question whether Al and Si are isotropically incorporporated into the aluminosilicate structure or if the Al shows a preference for certain sites. Since Al introduces negative charge into the lattice, one could, on one hand, expect Al-occupied sites in the aluminosilicate to be close to TPA cations, already at the start of the self-assembly. On the other hand, it may be unfavorable for Al to enter relatively hydrophobic, purely siliceous precursor structures "statistically" formed at the high Si/Al ratio around a TPA−OH ion pair. In that case, Al would become incorporated at a later stage and be located more at the outside of the siliceous entity. The syntheses were performed using TEOS, TPA−OD, and D_2O to suppress the possible effect of water and silanol protons on the ^{1}H−^{29}Si NMR distance measurements. ^{1}H−^{29}Si CP MAS NMR suggests the TPA template is in close contact with the silica. The observed effective H_{TPA}−Si and H_{TPA}−Al distances estimated from ^{1}H−^{29}Si and ^{1}H−^{27}Al rotational echo double resonance (REDOR) NMR experiments are compared with the distances derived from the computational model of the proposed precursor structures. The results support the encapsulation of the TPA molecule in the silicate shell of the precursor, which already has characteristics of the MFI framework topology.

Experimental Section

Synthesis. An amount of 0.018 g of Al metal powder (Acros, 99.9%) was oxidized in 6.1 g of a 40 wt % TPAOD in D_2O solution. The 40 wt % TPAOD in D_2O solution was prepared through the elution of a 0.1 N TPABr (Acros, 99%) in D_2O (Sigma, 99.8 atom % D) solution over an anion-exchange resin (Amberlite IRA-400) in the OD form and evaporating the excess D_2O at 50 °C under reduced pressure. An amount of 6.917 g of TEOS (Acros, 98%) was hydrolyzed in the TPAOD−aluminate solution to obtain a precursor solution with a Si/Al ratio of 50:1.

To prepare the precursor powder sample (1), part of this mixture was cooled in liquid nitrogen and freeze dried using a Christ Alpha 1-2 apparatus. A white powder was obtained.

To obtain the nanoslabs (2), TPAOD was generated from the reaction between TPABr in D_2O and Ag_2O. After filtration, the solution was stirred for 30 min to ensure TEOS hydrolysis and D_2O was then added (same proportion as sample 3). The solution was stirred at RT for 24 h before measurement. Thereafter, the solution was kept at +4 °C until the NMR measurements.

To synthesize the colloidal ZSM-5 sample (3), 3.48 g of D_2O were added to 6.52 g of the same precursor solution as for (1), 10 min after TEOS hydrolysis. This solution was stirred for 24 h at 25 °C. The solution was subsequently heated in a glass flask at 120 °C for 24 h. The solids formed were separated by centrifugation at 12 000 rpm during 15 min and washed by adding amounts of 75 mL of D_2O and repeating centrifugation until the pH of the washing water was below 9. Finally, the powder was freeze dried.

NMR. All NMR spectra were recorded on a Bruker DMX500 NMR spectrometer operating at a ^{29}Si NMR frequency of 99 MHz. The respective^{13}C and ^{27}Al NMR frequencies were 125 and 130 MHz. Standard Bruker MAS probeheads were used with rotor diameters of 7 mm and 4 mm. The frozen sample (2) was rotated in a 7-mm sample holder at a rate of 3 kHz, and the temperature was kept at 210 K. The freeze-dried sample (1) and the multicrystalline powder sample (3) were measured at room temperature in 4-mm rotors spinning at a MAS rate of 15 kHz. The π-pulses on ^{13}C, ^{27}Al, ^{29}Si, and ^{1}H nuclei were adjusted to 10 μs. Quantitative ^{29}Si and ^{13}C NMR spectra were recorded by direct excitation with a single 45° pulse and sufficiently long interscan delays, typically 600 s for ^{29}Si NMR and 20 s for ^{13}C NMR. Quantitative ^{27}Al NMR spectra were recorded with a single pulse of 2 μs. In ^{29}Si-{^{1}H} and ^{27}Al-{^{1}H} REDOR experiments, the initial ^{29}Si and ^{27}Al magnetization was, respectively, generated by ^{1}H−^{29}Si and ^{1}H−^{27}Al cross-polarization before the train of π-pulses on the proton channel was applied. MQMAS ^{27}Al NMR spectra with a zero-quantum filter were recorded by use of the three-pulse sequence $p_1-t_1-p_2-\tau-p_3-t_2$ with strong pulses $p_1 = 3.0$ μs and $p_2 = 1.2$ μs at a radio frequency field strength of 150 kHz and a weak pulse $p_3 = 11$ μs at a field strength of 7 kHz. The evolution time t_1 was sampled with 64 time increments of 20 μs, the signal was recorded during t_2 with a sample time of 10 μs up to 10.3 ms, and the filter time τ was 20 μs.

Computation. DFT calculations of the precursor model were performed using the Amsterdam Density Functional (ADF) program (ADF2002.03, SCM, Theoretical Chemistry, Vrije Universiteit, Amsterdam, The Netherlands, http://www.scm.com), in which Slater-type functions are used to represent atomic orbitals. The basis sets employed were of the double-ζ quality. To reduce computational costs, the following inner core orbitals were kept frozen: 1s for C, N, and O and up to 2p for Si. The RPBE exchange[26] and PBE correlation[27] gradient-corrected (GGA) functionals were used throughout. The model has a formula $[Si_{35}O_{87}H_{34}{\cdot}C_{12}H_{28}N]^+$, which represents a Si35 precursor. To simulate the effect of TPA cations bound to the external precursor surface, the silanol protons at 8 of the 20 Q^3 sites in the proposed P35 structure were replaced with TPA cations. The resulting precursor−TPA complex, P35−$(TPA)_9$, was optimized by an iterative procedure of energy minimizations and molecular-dynamics simulations with default force-field parameters within the program ChemBats3D Ultra Version 5.0 from CambridgeSoft (products.cambridgesoft.com).

Results

The TPA-directed synthesis of ZSM-5 from tetraethoxysilane (TEOS) at low levels of aluminum hydroxide cations is a

TABLE 1: Molar Ratios Estimated from Quantitative ^{1}H, ^{13}C, ^{27}Al, and ^{29}Si NMR

	synthesis	sample 1	sample 3
H/C	2.3	4.3	3.4
C/Si	4.3	4.2	0.7
Si/Al	50	62	38

delicate pH- and temperature-dependent process. Before starting detailed NMR distance measurements to characterize the dispersion of TPA within the aluminosilicate species formed at various stages during the synthesis, we have therefore checked the composition of the systems with multinuclear NMR spectroscopy. Freeze-dried precursor (sample 1) and the final TPA-ZSM5 (sample 3) were studied with MAS ^{13}C, ^{29}Si, ^{27}Al, and ^{1}H NMR. By comparing the signal intensity in various quantitative NMR spectra with the reference compounds (1,3,5,7,8,11,13,15-octakis-(dimethylsilyloxy)penta-cyclo-(9.5.1.1.^{3,9}1.^{5,15}1^{7,13}) octasiloxane (Aldrich 97%) and α-Al_2O_3), we estimate the respective atomic ratios and compare these with those at the synthesis (Table 1).

The estimated H/C ratios from the NMR spectra indicate that, apart from TPA ($C_{12}H_{28}N^+$), there are also inorganic protons present in the deuterated sample, like HDO. The C/Si ratio for sample 1 reflects a 12-fold excess of TPA cations relative to the proposed precursor structure consisting of 35 T sites and one enclosed TPA cation. In the proposed synthesis mechanism, an excess of externally attached TPA is indeed needed to stabilize the precursor particles and prevent these from further condensation. As expected, the C/Si ratio for the final zeolite (sample 3) is smaller. For four TPA ions per unit cell, $|((C_3H_7)_4\text{-}NOH)_4|$ $[Si_{95.7}Al_{0.3}O_{192}]$, the value would be 0.5, which is close to the value of 0.7 actually found. The Si/Al ratio of ~62 for sample 1 is higher than expected from the synthesis conditions (Si/Al = 50), whereas this ratio for sample 3 is lower. This may suggest that Al is not isotropically incorporated into the precursor structures formed around the TPA cations or TPA−OD ion pairs. However, there may be a significant error in the external reference procedure, especially for ^{27}Al with its quadrupolar properties and ^{29}Si with its generally long relaxation times in silicates. $^{1}H-^{13}C$ cross-polarization spectra at short contact times show the three ^{13}C NMR signals of TPA (Figure 1). The signals of the precursors are broader than those of the final zeolite, probably as a result of homogeneous and inhomogeneous mechanisms. The methyl signal of sample 3 shows the familiar splitting, explained by the position of TPA at the cross-sections between the zigzag and straight channels in MFI.[28] Direct-excitation Hahn-echo ^{13}C NMR spectra show two additional sharp signals at 17 and 55 ppm. The fact that these are not visible in the CP spectra indicates they belong to a mobile compound. Comparing with liquid-state spectra of TPA in water, ethanol, and TEOS, we assign these to a minor fraction of ethanol still present after freeze drying. A small, but significant, signal at 22 ppm may arise from a small amount of tripropylamine, formed by Hofmann degradation of TPA.

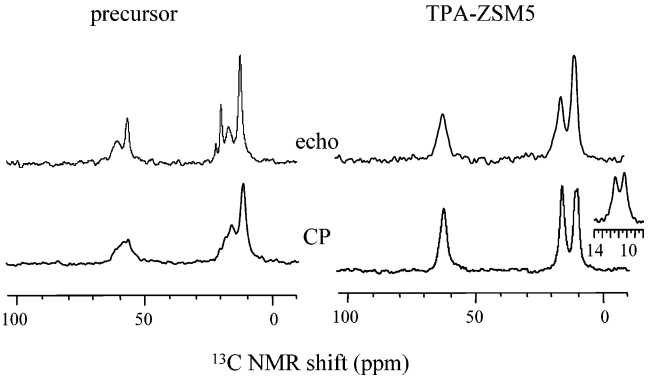

Figure 1. MAS ^{13}C NMR spectra of precursor (sample 1): (lower) $^{1}H-^{13}C$ cross-polarization spectrum with a contact time of 1 ms emphasizing the immobilized TPA fraction and (upper) Hahn-echo spectrum.

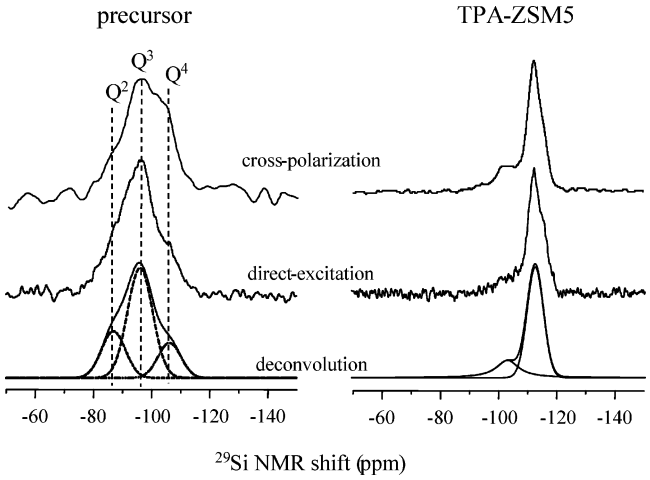

Figure 2. MAS ^{29}Si NMR spectra of the precursor (sample 1) and final TPA-ZSM5 (sample 3): (upper) cross-polarization, (center) quantitative direct excitation, and (lower) deconvolution.

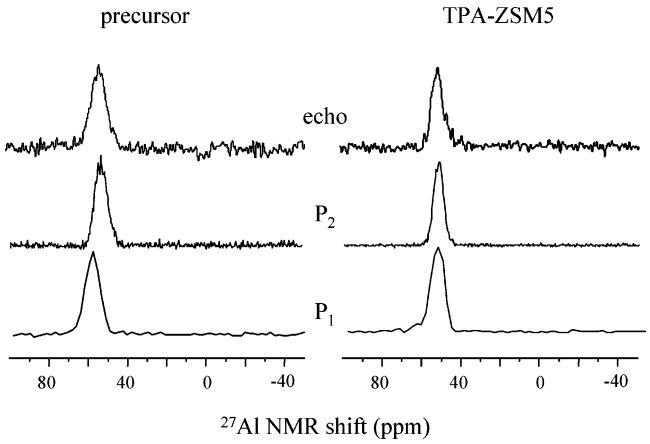

Figure 3. One-dimensional ^{27}Al NMR echo spectra and P_1 and P_2 projections of two-dimensional MQMAS spectra of the precursor and final TPA-ZSM5.

CPMAS ^{29}Si NMR spectra are readily obtained for all three D_2O-exchanged samples (Figure 3), indicating that most silicon atoms are in the direct vicinity (<1 nm) of TPA protons. The cross-polarization and direct-excitation spectra of sample 3 are closely similar. The major signal at approximately −112 ppm is associated with $Q^4 = [Si(OSi)_4]$ type silicon, that is, silicon with four silicon neighbors in the second coordination sphere, as in a completely condensed silicate. The weaker, hardly resolved, signals between −90 and −100 ppm are due to Si with Al or H in the second coordination sphere, like $Q^3 = [Si(OSi)_3(OH)]$ or $[Si(OSi)_3(OAl)]$. Deconvolution of the ^{29}Si NMR line shows that Q^2 and Q^3 represent ~20% of the total silicon species. This indicates that sample 3, that is, the colloidal TPA-ZSM5 material, is largely (although not completely) condensed. In contrast, the direct-excitation ^{29}Si NMR spectrum of sample 1 shows a much lower condensation degree, indicating small silicate species or a rather open silica structure. The direct-excitation ^{29}Si NMR line of sample 1 has a maximum at −96 ppm but further no clear discontinuities or shoulders, which can

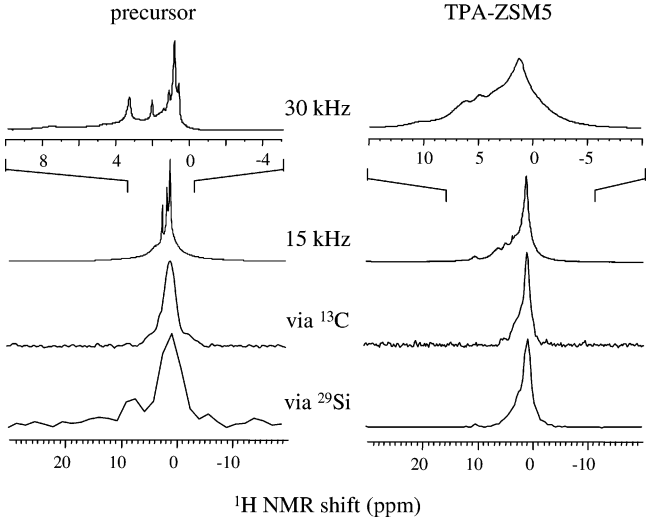

Figure 4. MAS ^{1}H NMR spectra of the precursor (sample 1) and final TPA-ZSM5 system (sample 3): (1st and 2nd rows) direct-excitation 30- and 15-kHz MAS spectra reflecting all proton-containing species in a quantitative way; (3rd row) ^{1}H projection from a 2D ^{1}H-^{13}C NMR spectrum representing the rigid TPA fraction and (4th row) from a 2D ^{1}H-^{29}Si NMR spectrum reflecting the rigid species closely around the silicon atoms. 2D NMR spectra were recorded at a MAS rate of 15 kHz.

be unambiguously interpreted as discrete Q^2, Q^3, or Q^4 sites (Figure 2). Assuming that the same components, albeit with different intensity, underlie the ^{1}H−^{29}Si cross-polarization NMR spectrum, we have made a coupled deconvolution in terms of three Gaussian signals. The fit results suggest that the precursor sample exists of 23% Q^2, 61% Q^3, and 16% Q^4. This reasonably agrees with the ratio of 12:72:15 expected for the 33-T precursor proposed by Martens and Kirschhock. It is difficult to reconcile with Knight and Kinrade's cubic octamers, which contain Q^3 sites only, unless the precursor sample would consist of a mixture of octamers and higher condensed silica structures.

Both the precursor sample and the final TPA-ZSM5 zeolite contain a small amount of aluminum, Si/Al $\sim$ 50 (between 38 and 62, as estimated with NMR). Since ^{27}Al is a quadrupolar nucleus, its NMR signal broadens under the influence of electric field gradients arising from a nonisotropic charge distribution around the Al position. Magic-angle spinning alone is unable to completely remove this quadrupolar broadening from the ^{27}Al NMR spectrum. Multiple-quantum (MQMAS) NMR, however, allows us to distinguish between quadrupolar- and other line-broadening mechanisms. After proper processing of the 2D spectra, the projection P_1 on one of the two frequency axes is free of quadruplar line broadening. The other projection P_2 on the direct axis tends to be similar to the 1D MAS ^{27}Al NMR spectrum. For both samples, we observe an ^{27}Al NMR shift value of 53 ppm both in the 1D spectra and in the P_2 projections (Figure 3). This indicates that aluminum is incorporated with tetrahedral oxygen coordination into the zeolite framework already at an early stage in the self-assembly. The ^{27}Al NMR line width in the P_1 projections is the same as in the P_2 projection (Figure 3). Thus, the MAS ^{27}Al NMR line width is mainly dominated by chemical-shift heterogeneity, for example, associated with slight conformation differences among the T sites.

Direct-excitation ^{1}H NMR spectra contain the three narrow signals characteristic of a mobile fraction, as well as broad components mainly associated with immobilized molecules (Figure 4). Judging from the chemical-shift positions, the most evident species in the mobile fraction are ethanol molecules but there also some narrow signals from mobile TPA. The ^{1}H projection of the two-dimensional cross-polarization-based ^{1}H−^{13}C NMR spectrum shows proton signals of the immobilized TPA fraction only (Figure 4). Even broader ^{1}H NMR signals are present in the ^{1}H projection of CP-based ^{1}H−^{29}Si correlation spectra (Figure 4), indicating that rigidly bound TPA is close to the silicon atoms. More mobile TPA cations or ethanol could also be close, but these would not easily show up in this type of CP-based experiment. A minor signal in the ^{1}H projection at ca. 9 ppm cannot be ascribed to TPA protons and may be assigned to N−H−O bridges between silanol positions and tripropylamine molecules. Seemingly, despite all synthetic precautions, not all silanol protons have been completely replaced by deuterons or some back exchange has occurred upon exposure of the sample to air.

To obtain detailed information on the precursor geometry, we have carried out NMR distance measurements by use of the so-called REDOR technique on various spin combinations, such as ^{13}C-{^{29}Si}, ^{27}Al-{^{1}H}, and ^{29}Si-{^{1}H}. The dipole coupling between nuclear spins is inversely proportional to the cube of the internuclear distance and therefore, a valuable source of structure information. REDOR is based on a selective reintroduction of heteronuclear dipole interactions under MAS conditions by a rotor-synchronized train of π-pulses, typically on the nonobserved spin species, in our case the protons.[30] The resulting transverse-magnetization decay is compared with the "background" decay without these π-pulses and any significant difference interpreted in terms of a dipolar coupling constant. As a potentially interesting experiment, technically feasible in our lab, we have carried out ^{13}C-{^{29}Si} REDOR because of the high chemical resolution in the ^{13}C dimension. The dipole interaction between ^{13}C and ^{29}Si is weak, and their natural abundance is low, 2 and 5%, respectively. Nevertheless, with 35 Si atoms in the proposed precursor structure, any ^{13}C nucleus at one of the C positions in TPA would typically "see" one or two ^{29}Si nuclei in its direct vicinity. Indeed, we observe significant ^{13}C-{^{29}Si} REDOR effects for the final TPA-ZSM5 (sample 3, not shown), consistent with a close encapsulation of the TPA cations in the silica phase. However, we are unable to record significant ^{13}C-{^{29}Si} REDOR effects for the precursor (sample 1) at the short time scale, T_{2e}, of its ^{13}C Hahn-echo decay without proton π-pulses. In contrast, ^{29}Si−^{1}H dipole interactions tend to be stronger because of the larger gyromagnetic ratio of protons as compared to ^{13}C nuclei, $\gamma_H/\gamma_C \sim 4$, and the ^{29}Si spin lifetime for our samples is fairly long (>20 ms). This permits the measurement of the weak ^{29}Si−^{1}H dipole interactions in ^{29}Si-{^{1}H} REDOR experiments. The disadvantage of using ^{29}Si-{^{1}H} REDOR for studying distances in the TPA−silica structures is the manifold of simultaneous interactions between a given ^{29}Si nucleus in the lattice and the 28 protons of TPA. Fortunately, the strong distance dependence of the dipole interaction acts as a spatial filter.

The ^{29}Si-{^{1}H} REDOR results for the three systems, as well as the reference compound methyl-silsesquioxane (T8M8), are shown in Figure 5. The reference compound T8M8 has a cubic molecule structure with methyl groups attached to Si at the corners connected by O in the ribs and therefore represents an illustrative sample of fairly isolated ^{29}Si−^{1}H$_3$ spin clusters. None of the curves shows the damped oscillatory behavior expected for isolated spin pairs. T8M8 with its well-defined ^{29}Si−^{1}H distance of 2.47 Å shows the fastest REDOR. The REDOR curve observed for the final TPA-ZSM5 sample (3) resembles that for the Q^4 component of the precursor and nanoslab samples 1 and 2. This confirms the picture that, in addition to externally attached TPA, there are also TPA cations embedded inside the

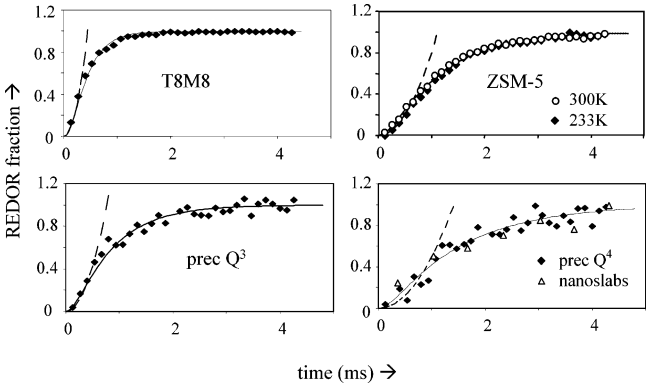

Figure 5. ^{29}Si-{^{1}H} REDOR curves for the reference compound methyl-silsesquioxane (T8M8), the final TPA-ZSM5, and the Q^3 and Q^4 components in the lineshape fit of the ^{29}Si NMR spectrum of the precursor. The parabola fit to the initial part of the curve below REDOR fraction <0.4 is indicated with a broken line. The continuous curve represents the Anderson−Weiss fit $1 - \exp[-(32/15)M_2\tau_c^2\{\exp(-t/\tau_c) - 1 + t/\tau_c\}]$.

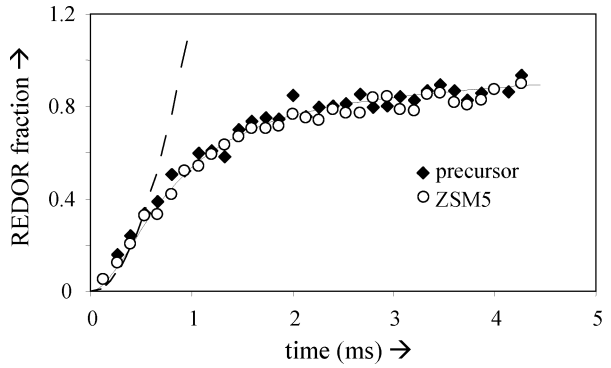

Figure 6. ^{27}Al-{^{1}H} REDOR curves for the final TPA-ZSM5 and the precursor. The parabola fit to the initial part of the curve below REDOR fraction <0.4 is indicated with a broken line. The continuous curve represents a superposition of two Anderson−Weiss curves.

precursor and the nanoslabs in a similar way as in the final zeolite. Since the nanoslabs have less external surface than the precursor species, the comparable REDOR curves indicate that TPA is also internally located in the precursor and nanoslabs. The Q^3 line shape component of the precursor shows faster REDOR behavior, indicating that, on average, the Q^3 sites are effectively closer to the TPA protons than the Q^4 sites in the precursor. A possible explanation would be that the Q^3 signal largely represents the silanol positions in the precursor particles. At the high pH necessary to stabilize the precursor particles, these silanols are deprotonated and attract TPA cations. This yields a locally enhanced proton density around the Q^3 sites relative to that around the Q^4 sites inside of the precursor and the fully condensed final zeolite.

^{27}Al-{^{1}H} REDOR could be readily observed for both the precursor and the final TPA-ZSM5 sample. The observed ^{27}Al-{^{1}H} REDOR are closely similar (Figure 6), which is consistent with the hypothesis that the TPA cations are already taking their final positions quite early in zeolite synthesis.

Discussion

The NMR spectra in the Results section show that the aluminasilicate species formed at an early stage in our synthesis procedure have a higher condensation degree than expected for the cubic octameric silicate polyanions proposed by Knight and Kinrade[22,23] but lower than that expected for the (dense) silica nanoparticles proposed by other groups.[24,25] The $Q^2/Q^3/Q^4$ ratio is consistent with the 33-T precursor proposed by Martens and Kirschhock.[18−20] Already, at an early stage, aluminum is incorporated with tetrahedral oxygen coordination into the precursor. The effective ^{1}H−^{29}Si cross-polarization observed in our experiments is indicative for intimate contacts between the TPA and the aluminasilica species formed. Such contacts would not arise from silica nanoparticles with only externally attached TPA but are consistent with the 33-T precursor model, which contains one TPA cation in the center. The different ^{13}C NMR spectra for samples 1 and 3 indicate that the location and dynamics of TPA attached to the early aluminosilicate species are not the same as in the final zeolite. This is not surprising because, in addition to the TPA cation supposedly located in the center of the 33-T precursor in a way similar to in the final zeolite, there is an excess of TPA attached to the external precursor surface in order to prevent it from further condensation.

One of the main issues in the scientific debate about the MFI-synthesis mechanism is whether the TPA is encapsulated within the early silicate species or only attached to the external surface. In this respect, solid-state NMR is a powerful technique, since it allows atomic distances to be measured in systems without long-range order. A specific NMR technique, which combines high chemical resolution in magic-angle-spinning experiments with the distance information from dipole interactions, is the so-called REDOR experiment. In particular, for isolated pairs of NMR-visible nuclei in a molecule, this technique yields accurate distances.[29] The interpretation of REDOR behavior for systems more complex than an isolated, rigid spin pair has been widely discussed in the literature.[30−33] Strong homonuclear coupling in the proton subsystem,[30] zero-quantum relaxation,[34] and imperfections of the experimental setup[35] make the situation even more complicated. Several new approaches have been developed recently to cope with these problems.[31,33,36,37] However, none of these was sufficiently robust for our samples with their limited signal-to-noise ratios and coherence lifetimes. We therefore rely on the effective distance information we can still extract from the basic REDOR curves. For "ill-defined" structures with multiple spin interactions, like in glasses, Bertmer and Eckert propose to focus at the *initial* behavior of the REDOR curve.[32] The initial REDOR curve of an observed spin I coupled to a number of S spins is approximately *parabolic*

$$R(t) = ({}^{16}/_{15})\, M_2 t^2 = 1.067 \sum D_k^2 t^2 \qquad (1)$$

with $M_2 = \sum D_k^2$, the cumulative second moment of the various dipolar IS_k couplings D_k. Since the dipolar coupling decreases with the cube of the distance, $D_k = Cr_k^{-3}$ with $C = 24$ kHz Å^3 for ^{27}Si−^{1}H interactions; the M_2 is dominated by the shortest distances. Beyond the initial range, the REDOR behavior depends on the exact configuration/geometry of the spin manifold. The values obtained from a parabolic fit to the initial REDOR curves below fraction 0.4 are indicated in Table 1.

To interpret these fit values, we have used the proton-intrapolated crystal structure of TPA-ZSM5 and derived the Si−H distance distribution $g(r_{ik})$ between the 12 inequivalent silicon positions i within a unit cell and the 284 proton positions k from TPA cations in a cube of $5 \times 5 \times 5$ unit cells around these silicon atoms.[38] Above a certain minimum distance r_{min}, the proton density $g(r)$ as a function of r resembles that of a continuous medium $g(r) = \rho r^2$ with ρ being the average number of protons per volume unit, that is, 116 per unit cell. Since the cumulative second moment, $M_2 = C^2 \sum (r_{ik})^{-6} \sim C^2 \int g(r) r^{-6}\, dr$ is dominated by the nearest distances, however, the discrete character of the crystal structure cannot be neglected.The M_2

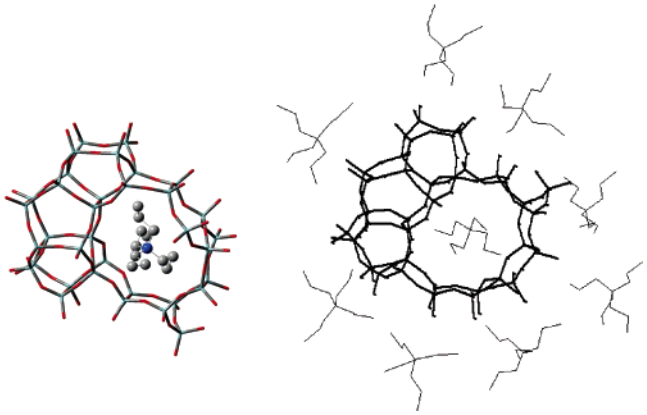

Figure 7. (left) DFT-optimized structure of the proposed precursor P35; (right) MM-optimized structure of a partly deprotonated P35 structure with one encapsulated TPA and eight TPA cations at the external surface.

TABLE 2. Comparison of Theoretical M_2 Values and M_2 Values Estimated from an Initial Parabola Fit and an Anderson−Weiss Fit to ^{29}Si-{^{1}H} REDOR Curves

	modeling		parabola fit		Anderson−Weiss	
	M_2 (kHz^2)	r_{eff} (Å)	M_2 (kHz^2)	r_{eff} (Å)	M_2 (kHz^2)	τ_c (ms)
T8M8	7.55	2.47	5.0	2.64	7.6	0.11
ZSM5-TPA	1.88	2.60	0.83	2.99	1.9	0.13
precursor Q^3	1.61	2.67	1.23	2.79	3.3	0.10
precursor Q^4	1.51	2.70	0.65	3.11	1.5	0.12

value for every silicon atom in the lattice is mainly, although not completely, determined by the minimum distance r_{min} to the closest proton (Table 3). Similarly, using a combination of quantum- and classical-mechanical computation techniques we have calculated the Si−H distance distribution in the proposed precursor P35 with one internal TPA inside and 8 TPA cations at the external surface compensating the negative charges of 8 deprotonated silanol moieties, arbitrarily selected from the 20 Q^3 positions. The resulting average Si−H distance distribution indeed indicates a difference between the Q^3 and Q^4 sites in the precursor particles but relatively smaller than that observed from the REDOR curves (Table 2). The resulting average M_2 values per NMR-distinct silicon-type Q^2, Q^3, and Q^4 are compared with the initial curvature estimated from the parabolic fit to the experimental REDOR curves in Table 2.

The ^{1}H−^{29}Si coupling for precursor Q^4 and ZSM5 is weaker then expected from the rigid model structure. The second moments M_2 extracted from the experimental REDOR curve are both a factor ∼2.3 smaller than those theoretically predicted. This could indicate a systematic cause, such as motional averaging of the dipole interactions by internal TPA motion. However, there is no temperature effect. Moreover, a similar scaling is also observed for the crystalline T8M8 reference compound, which should be perfectly rigid. We therefore explain the reduction of the effective ^{29}Si−^{1}H dipole coupling by a multispin phenomenon called "self-decoupling", also observed for ^{13}C−^{1}H coupling in, for example, polymers.[39−41] The magnetization exchange between protons as a result of spin diffusion has a similar narrowing effect on the ^{13}C−^{1}H coupling as rotational motion. For a semiquantitative description, we follow the approach of Anderson and Weiss[42] (AW) and Abragam.[43] The first have developed a statistical-mechanical model for the behavior of spins with stochastically fluctuating dipole interactions in the presence of exchange. The latter has adapted this for spins in a fluctuating local magnetic field. These fluctuations are generally interpreted in terms of mobility, but here we propose that these also manifest themselves in a static system as a result of the coupling of the spin system to the outside world. In general, the lack of perfect isolation causes a leakage of coherence from the spin pair into the multispin environment. Since this leakage affects the transverse magnetization of the observed spins, for example, ^{29}Si, only *indirectly* through the averaging of the dipole Hamiltonian, and basically has a *coherent* nature, we call it "decoherence", rather than "dephasing" or "relaxation". The standard REDOR decay for isolated spin pairs *IS* with nonfluctuating dipole interactions involves an average dipole Hamiltonian $H_{IS} = h\omega_{IS}(\Omega)2I_zS_z$ with the effective dipolar frequency $\omega_{IS}(\Omega) = -2\sqrt{2}D \sin 2\beta \sin \gamma$ depending on the dipole coupling constant D and the static orientation (β,γ) of the internuclear vector *IS* with respect to the sample holder. The REDOR decay $I(t)$ then equals the average $\langle\cos[\omega_{IS}(\Omega)t]\rangle$ over all orientations. For weakly coupled ^{29}Si−^{1}H pairs with strong coupling between its proton and the surrounding protons, however, noncommuting perturbation terms H_{pert} in the Hamiltonian cause a modulation of the dipole Hamiltonian. After a convenient transformation $U(t) = \exp(iH_{pert}t/h)$ and projection P from multispin space onto two-spin space *IS*, the REDOR Hamiltonian is of the form $H_{IS}^*(t) = h\omega_{IS}(\Omega)c(t)\ 2I_zS_z$, where $c(t)$ represents the modulation by the spins in the environment. We now assume that for a multispin system without statistic correlation between H_{IS} and H_{pert}, $c(t)$ behaves as a Gaussian stochastic variable with vanishing average $\langle c(t)\rangle = 0$, normalized second moment $\langle c^2(t)\rangle = 1$, and stationary correlation function $g(\tau) = \langle c(t+\tau)c(t)\rangle$ independent of time t. Also approximating $\omega_{IS}(\Omega)$ as a Gaussian parameter statistically independent of $c(t)$, and using the ensemble average property for Gaussian variables X, $\langle\cos X\rangle = \exp(-\langle X^2\rangle/2)$, we obtain for the REDOR decay

$$\begin{aligned} I(t) &= \langle\cos[\omega_{IS}(\Omega)\int_0^t c(t')\,dt']\rangle \\ &= \exp[-\langle\omega_{IS}{}^2(\Omega)\rangle\langle\{\int_0^t c(t')\,dt'\}^2\rangle/2] \\ &= \exp[-\langle\omega_{IS}{}^2(\Omega)\rangle\int_0^t (t-\tau)g(\tau)\,d\tau/2] \end{aligned} \qquad (2)$$

For a simple monoexponential decay $g(\tau) = \exp(-\tau/\tau_{dc})$, where the "decoherence time" τ_{dc} reflects the time scale at which the spin pair cannot be treated isolated from the environment, this reduces to

$$I(t) = \exp\left[-\frac{32}{15}M_2\tau_{dc}{}^2\{e^{-t/\tau_{dc}} - 1 + t/\tau_{dc}\}\right] \qquad (3)$$

where we have substituted $\langle\omega_{IS}{}^2(\Omega)\rangle$ by $(^{64}/_{15})M_2 \sim 4.267\ \sum D_k{}^2$, so that the roughly Gaussian behavior at short time $t < \tau_{dc}$, $I(t) \sim \exp[-(^{16}/_{15})M_2t^2]$, is consistent with eq 1. For large times $t > \tau_{dc}$, $I(t)$ approaches the exponential function $1 - R\exp[-(^{32}/_{15})M_2\tau_c t]$ with $R = \exp[(^{32}/_{15})M_2\tau_c{}^2]$. The latter may be compared with REDOR in the presence of fast zero-quantum relaxation.[35] The AW model is often used to describe proton transverse-magnetization decays in rubber polymers.[44] Despite its success as a phenomenological description, its validity for rubbers has been criticized, especially the tacit assumption of isotropic polymer-chain motion, which is physically unrealistic for these systems.[45] Perhaps combined anisotropic chain motion and self-decoupling explain the success of the AW curve as a fit model.

The ^{29}Si-{^{1}H} REDOR curves, we have observed in the present study, are also well described by the AW model (Figure

TABLE 3: Calculated Values for $M_2 = C^2 \sum (r_{ik})^{-6}$, the Effective Si−H Distance $r_{eff} = [\sum (r_{ik})^{-6}]^{-1/6}/N$, and the Minimum Si−H Distance r_{min} for the 12 Inequivalent Si Positions in ZSM5-TPA and the 20 Q^3 and 7 Q^4 Positions in the Precursor P35

ZSM5-TPA

	Si1	Si2	Si3	Si4	Si5	Si6	Si7	Si8	Si9	Si10	Si11	Si12	average
M_2 (kHz^2)	2.09	1.93	1.94	1.40	2.07	1.99	1.68	1.60	2.05	1.84	1.90	2.01	1.88
r_{eff} (Å)	2.29	2.35	2.35	2.61	2.29	2.32	2.46	2.50	2.30	2.39	2.36	2.32	
r_{min} (Å)	3.08	3.32	3.45	3.47	3.33	3.41	3.47	3.18	3.30	3.40	3.05	3.08	

precursor Q3

	Si1	Si2	Si3	Si4	Si5	Si6	Si7	Si8	Si9	Si10	average
M_2 (kHz^2)	1.63	0.98	1.32	0.57	0.64	1.12	1.75	2.19	2.40	1.83	1.61
r_{eff} (Å)	2.48	2.94	2.67	3.53	3.39	2.81	2.43	2.25	2.18	2.39	
r_{min} (Å)	3.00	3.58	3.19	4.20	4.27	3.36	3.01	2.86	2.70	2.80	

	Si11	Si12	Si13	Si14	Si15	Si16	Si17	Si18	Si19	Si20
M_2 (kHz^2)	2.00	1.96	1.81	2.05	0.85	1.61	1.94	1.87	1.11	0.45
r_{eff} (Å)	2.32	2.34	2.40	2.30	3.09	2.49	2.34	2.37	2.82	3.81
r_{min} (Å)	3.20	3.16	3.08	3.16	4.03	2.95	2.91	3.02	3.34	5.71

precursor Q4

	Si1	Si2	Si3	Si4	Si5	Si6	Si7	average
M_2 (kHz^2)	1.87	1.87	0.75	1.38	1.69	1.80	0.68	1.51
r_{eff} (Å)	2.37	2.37	3.22	2.63	2.46	2.40	3.32	
r_{min} (Å)	2.67	3.03	4.25	3.09	2.92	2.99	4.82	

6). The lack of temperature dependence observed for the final TPA-ZSM5 zeolite practically excludes motion as the cause of the averaging and confirms our view that complex multispin effects, or self-decoupling, can cause a similar effect. The AW model offers a good fit to the curve as a whole and provides a way to estimate the second moment M_2 of the dipole interaction from the *complete* REDOR curve, rather than the first few data points (eq 1). The sampling rate of the REDOR curve is limited to multiples of the sample rotation time, so that there is a maximum to the number of REDOR data to be recorded sufficiently close to 0. Fitting the observed REDOR, we observe that various combinations of M_2 and τ_{dc} yield a similar standard deviation. The reason is that most curves seem to transit from coherent Gaussian behavior to incoherent exponential behavior within the first few data points; that is, they practically follow the exponential $I(t) \sim 1 - R \exp[-(32/15)M_2\tau_{dc}t]$, which, when $M_2\tau_{dc}^2 \ll 1$, is fairly invariant for coupled changes in M_2 and τ_c. Instead of fitting with M_2 and τ_c as free parameters, we therefore tried fixing M_2 to the computed value resulting from the modeling. In this way, we actually test whether the rigid theoretical model is still acceptable, if one introduces decoherence characterized with a correlation time τ_{dc} as an averaging effect. This procedure works fine for the reference compound T8M8 with its known Si−H distance of 2.47 Å, the Q^4 sites in the precursor, and the final TPA-ZSM5 zeolite. It is remarkable that without any other fit constraint than fixing M_2 to the theoretically predicted value, all τ_{dc} values end up being on the order of 0.1 ms (Table 2). This value is smaller than the REDOR sampling time at the MAS rate of 15 kHz, which explains the lack of any clearly observed parabolic initial behavior. The physical interpretation of τ_{dc} still puzzles us. Its value could indicate the proton spin diffusion rate and indeed corresponds to the highest dipole constant of ∼8 kHz between protons at neighboring carbon positions in a TPA cation. It is unclear, however, how this relatively weak homonuclear coupling could survive 15-kHz MAS. For the Q^3 sites, fixing M_2 in the AW model (eq 3) to the theoretically expected value results in an unacceptable bad fit to the experimental REDOR data. The lowest value of M_2 which, in combination with $\tau_{dc} = 0.1$ ms, offers a good description, is ca. 3.3 kHz^2 corresponding to an effective Si−H distance of 2.36 Å. The Si−H distance in a protonated silanol moiety would be 2.17 Å, corresponding to a M_2 value of 5.5 kHz^2. Combined with the computed value of 1.66 kHz^2 for the deuterated or deprotonated Q^3 site, it seems that ca. 50% of the silanols are actually protonated. Given the excessive exchange against D_2O, this is a surprising outcome.

^{27}Al-{^{1}H} REDOR is approximately the same for both the precursor and the final zeolite. For Al isotropically substituted within the precursor structure, the expected values of the second moment M_2 are simply a factor $(\gamma_{Al}/\gamma_{Si})^2 \sim 1.7$ (with γ_{Al} and γ_{Si} being the gyromagnetic ratios for ^{27}Al and ^{29}Si) higher than those for the ^{29}Si-{^{1}H} curves (Table 1). Fitting a parabola to the initial curve yields a value of 1.2 kHz^2, corresponding to an effective Al−H distance of ∼3.1 Å. Like for the ^{29}Si-{^{1}H} REDOR curves, the initial curvature is weaker than expected on the basis of the precursor model. The observed curve cannot be described in terms of a single-component AW model. A good fit is obtained for a linear combination of two components with M_2 values of 5.7 kHz^2 (70%) and 0.9 kHz^2, both with a τ_c value of 0.3 ms. These M_2 values, respectively, correspond to Al−H distances of 2.36 and 3.22 Å. A distance of 2.36 Å is smaller than that expected from a model with Al isotropically distributed over the T-sites in the precursor structure. It could, however, indicate that part of the cation-exchange positions around Al-substituted sites in the lattice are occupied with a proton.

Conclusion

We have studied aluminosilicate species at three stages in the self-assembly of zeolite ZSM-5 with 1D- and 2D-MAS ^{13}C, ^{27}Al, ^{29}Si, and ^{1}H NMR spectroscopy and compared the results with the earlier proposed structures: (1) precursor species containing 33−36 T sites around a TPA cation, (2) nanoslabs consisting of a flat 4 × 3 array of such precursors, and (3) the final TPA-ZSM-5 zeolite. The condensation degree of the aluminosilicate species formed early in our synthesis, and the intimate TPA contacts with the species are consistent with the proposed 33-T precursor but difficult to reconcile with the cubic octamers or (dense) nanoparticles proposed in alternative models. To further determine the average TPA−aluminosilicate distances in more detail, we have carried out REDOR experiments on deuterium-exchanged systems. Under these conditions,

the effective Si−H and Al−H distances measured with ^{29}Si-{^{1}H} and ^{27}Al-{^{1}H} REDOR reflect the interactions between TPA cations and the aluminosilica. The close similarity between the ^{29}Si-{^{1}H} REDOR curves for Q^4-type silicon atoms at the three mentioned stages, as well as the similar ^{27}Al−^{1}H REDOR behavior curve for the precursor species compared to that for the TPA-ZSM-5, indicates that TPA is already incorporated at an early stage into the aluminosilicate in a similar way as in the final zeolite, in accordance with the earlier proposed MFI self-assembly pathway.[16] The fact that the initial REDOR behavior is weaker than that computed for the model is ascribed to a reduction of the ^{29}Si−^{1}H and ^{27}Al−^{1}H interactions by spin-decoherence effects. By assuming the computed model distances and fitting AW curves to the observed REDOR data, we obtain similar "decoherence times" in the order of 0.1 ms. The observed ^{29}Si-{^{1}H} REDOR dephasing for the Q^3 sites in the precursors is significantly faster than that for the Q^4 sites. This is tentatively ascribed to a partial deuteron-proton back exchange at the silanol positions.

Acknowledgment. The authors acknowledge the Belgian government for supporting the IAP-PAI interuniversity attraction poles program and Brahim Mezari for assisting in the NMR experiments.

References and Notes

(1) Flanigen, E. M.; Bennett, J. M.; Grose, R. W.; Cohen, J. P.; Patton, R. L.; Kirchner R. M.; Smith, J. V. *Nature* **1978**, *271*, 512.
(2) Chang, C. D.; Bell, A. T. *Catal. Lett.* **1991**, *8*, 305.
(3) Iton, L. E.; Trouw, F.; Brun, T. O., Epperson, J. E.; White, J. W.; Henderson, S. J. *Langmuir* **1992**, *8*, 1045.
(4) Burkett, S. L.; Davis, M. E. *J. Phys. Chem. B* **1994**, *98*, 4647; *Chem. Mater.* **1995**, *7*, 920.
(5) Persson, A. E.; Schoeman, B. J.; Sterte, J.; Otterstedt, J. E. *Zeolites* **1994**, *14*, 557.
(6) Regev, O.; Cohen, Y.; Kehat, E.; Talmon, Y. *Zeolites* **1994**, *14*, 314.
(7) Dokter, W. H.; van Garderen, H. F.; Beelen, T. P. M.; van Santen, R. A.; Bras, W. *Angew. Chem., Int. Ed. Engl.* **1995**, *34*, 73.
(8) Watson, J. N.; Iton, L. E.; Keir, R. I.; Thomas, J. C.; Dowling, T. L.; White, J. W. *J. Phys. Chem. B* **1997**, *101*, 10094.
(9) Watson, J. N.; Brown, A. S.; Iton, L. E.; White, J. W. *J. Chem. Soc., Faraday Trans.* **1998**, *94*, 2181.
(10) de Moor, P.-P. E. A.; Beelen, T. P. M.; Komansche, B. U.; van Santen, R. A. *Microporous Mater.* **1997**, *9*, 117.
(11) de Moor, P.-P. E. A.; Beelen, T. P. M.; van Santen, R. A. *J. Phys. Chem. B* **1999**, *103*, 1639.
(12) Schoeman, B. J.; Regev, O. *Zeolites* **1996**, *17*, 447.
(13) Schoeman, B. J. *Zeolites* **1997**, *18*, 97.
(14) Mintova, S.; Olson, N. H.; Senker, J.; Bein, T. *Angew. Chem.* **2002**, *114*, 2670.
(15) Schoeman, B. J. *Stud. Surf. Sci. Catal.* **1997**, *105*, 647.
(16) Kirschhock, C. E. A.; Buschmann, V.; Kremer, S.; Ravishankar, R.; Houssin, C. J. Y.; Mojet, B. L.; van Santen, R. A.; Grobet, P. J.; Jacobs, P. A.; Martens, J. A. *Angew. Chem., Int. Ed.* **2001**, *40*, 2637−2640.
(17) Ravishankar, R.; Kirschhock, C. E. A.; Knops-Gerrits, P. P.; Feijen, E. J. P.; Grobet, P. J.; Vanoppen, P.; De Schryver, F. C. E. A.; Miehe, G.; Fuess, H.; Schoeman, B. J.; Jacobs P. A.; Martens, J. A. *J. Phys. Chem. B* **1999**, *103*, 4960−4964.
(18) Kirschhock, C. E. A.; Ravishankar, R.; Van Looveren, L.; Jacobs, P. A.; Martens, J. A. *J. Phys. Chem. B* **1999**, *103*, 4972.
(19) Kirschhock, C. E. A.; Kremer, S. P. B.; Grobet, P. J.; Jacobs, P. A.; Martens, J. A. *J. Phys. Chem. B* **2002**, *106*, 4897.
(20) Houssin, C. J. Y.; Kirschhock, C. E. A.; Magusin, P. C. M. M.; Mojet, B. L.; Grobet, P. J.; Jacobs, P. A.; Martens, J. A.; van Santen, R. A. *Phys. Chem. Chem. Phys.* **2003**, *5*, 3518.
(21) Kirschhock, C. E. A.; Ravishankar, R.; Verspeurt, F.; Grobet, P. J.; Jacobs, P. A.; Martens, J. A. *J. Phys. Chem. B* **1999**, *103*, 4965.
(22) Knight, C. T. G.; Kinrade, S. D. *J. Phys. Chem. B* **2002**, *106*, 3329.
(23) Knight, C. T. G. *Zeolites* **1990**, *10*, 140.
(24) Fedeyko, J. M.; Vlachos, D. G.; Lobo, R. F. *Langmuir* **2005**, *21*, 5197.
(25) Caratzoulas, S.; Vlachos, D. G.; Tsapatsis, M. *J. Phys. Chem. B* **2005**, *109*, 10429.
(26) Hammer, B.; Hansen, L. B.; Norskov, J. K. *Phys. Rev. B* **1999**, *59*, 7413.
(27) Perdew, J. P.; Burke, K.; Ernzerhof, M. *Phys. Rev. Lett.* **1996**, *77*, 3865.
(28) Nagy, J. B.; Gabelica, Z.; Derouane, E. G. *Chem. Lett.* **1982**, 1105.
(29) Jaroniec, C. P.; Tounge, B. A.; Herzfeld, J.; Griffin, R. G. *J. Am. Chem. Soc.* **2001**, *123*, 3507.
(30) Goetz, J. M.; Schaefer, J. *J. Magn. Reson.* **1997**, *127*, 147.
(31) Gullion, T.; Pennington, C. H. *Chem. Phys. Lett.* **1998**, *290*, 88.
(32) Bertmer, M.; Eckert, H. *Solid State Nucl. Magn. Reson.* **1999**, *15*, 139.
(33) Chan, J. C. C. *Chem. Phys. Lett.* **2001**, *335*, 289.
(34) Costa, P. R.; Sun, B.; Griffin, R. G. *J. Magn. Reson.* **2003**, *164*, 92.
(35) Weldeghiorghis, T. K.; Schaefer, J. *J. Magn. Reson.* **2003**, *165*, 230.
(36) Saalwächter, K.; Schnell, I. *Solid State Nucl. Magn. Reson.* **2002**, *22*, 154.
(37) Jaroniec, C. P.; Tounge, B. A.; Herzfeld, J.; Griffin, R. G. *J. Am. Chem. Soc.* **2001**, 3507.
(38) Yokomori, Y.; Idaka, S. *Microporous Mesoporous Mater.* **1999**, *28*, 405.
(39) Spiess, H. W.; Haeberlen, U.; Zimmermann, H. *J. Magn. Reson.* **1977**, *25*, 55.
(40) Sinning, G.; Mehring, M.; Pines, A. *Chem. Phys. Lett.* **1976**, *43*, 382.
(41) Ernst, M.; Verhoeven, A.; Meier, B. H. *J. Magn. Reson.* **1998**, *130*, 176.
(42) Anderson, P. W.; Weiss, P. R. *Rev. Mod. Phys.* **1953**, *25*, 269.
(43) Abraham, A. *The Principles of Nuclear Magnetism*; Oxford University Press: London, 1961.
(44) Simon, G.; Baumann, K.; Gronski, W. *Macromolecules* **1992**, *25*, 3624.
(45) Saalwächter, K. *Macromolecules* **2005**, *38*, 1508.